Atomic force microscopy studies of SiGe films and Si/SiGe heterostructures

by M. A. Lutz R. M. Feenstra J. O. Chu

Atomic force microscopy (AFM) is used to study the topography of strained SiGe films and multilayer Si/SiGe heterostructures. Strain relaxation processes are found to determine the formation of surface morphology, with distinct morphological features arising from both misfit dislocation formation and threedimensional growth of coherent islands and pits on the surface. Studies of these features for various values of strain (Ge content) and growth temperature reveal the underlying physical processes determining the strain relaxation. Fourier analysis of AFM images is performed to obtain quantitative roughness information and to separate roughness components of different physical origin.

1. Introduction

In recent years the atomic force microscope (AFM) has been applied to a wide range of thin-film growth systems, with the surface morphology of the films often reflecting details of the governing growth processes. One particular application is the epitaxial growth of *strained* layers, in which the film and substrate materials have different lattice constants, a_t and a_s respectively, in the absence of strain. For *coherent* growth, in which the in-plane lattice constants of film and substrate are equal, the in-plane components of the strain $(\varepsilon_{\chi\chi}$ and $\varepsilon_{\gamma\gamma})$ equal the $\emph{mismatch}$ between film and substrate, $\varepsilon = (a_s - a_t)/a_t$. This strain, together with the growth temperature and possibly other parameters, determines the type of strain relaxation which occurs during growth. Figure 1 illustrates possible relaxation mechanisms. It is well known that coherently strained layers are unstable against roughening of the surface, or against three-dimensional (3D) growth of the film [1]. Modulation of the surface morphology or the formation of islands leads to a relief of elastic strain because of a slight difference in lattice constant between peaks and troughs of the corrugated surface, as indicated by vertical lattice planes in Figure 1. The relieved elastic strain energy competes with an increase in surface energy. An alternate means of strain relaxation, also shown in Figure 1, is the formation of misfit dislocations at the film/substrate interface. The amount of relieved strain by a linear density n_d of dislocations is $\Delta \varepsilon = b_m n_d$, where b_m is the misfit component of the Burgers vector. The energy gained by this strain relief is further proportional to the

^eCopyright 1995 by International Business Machines Corporation. Copying in printed form for private use is permitted without payment of royalty provided that (1) each reproduction is done without alteration and (2) the *Journal* reference and IBM copyright notice are included on the first page. The title and abstract, but no other portions, of this paper may be copied or distributed royalty free without further permission by computer-based and other information-service systems. Permission to *republish* any other portion of this paper must be obtained from the Editor.

0018-8646/95/\$3.00 © 1995 IBM

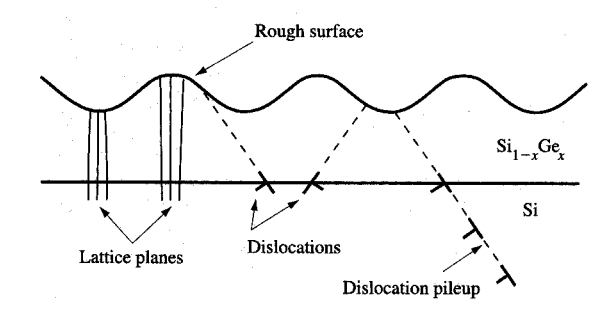


Figure 1

Schematic view of strain relaxation mechanisms for a thin film of $\mathrm{Si}_{1-x}\mathrm{Ge}_x$ on Si. Elastic relaxation occurs by means of the formation of a rough surface. Some vertical lattice planes are indicated by lines. Plastic relaxation occurs by means of dislocation formation. Glide planes for the dislocations are shown by dotted lines. Surface steps (not shown) occur where the glide planes intersect the surface. A pileup of dislocations with a common glide plane is indicated.

film thickness. In contrast, elastic strain relaxation by roughening is independent of film thickness. Thus, dislocation formation will always occur for sufficiently thick films. For thinner films, however, the transition between the two mechanisms depends in detail [2] on temperature, strain, and thickness, as described in this paper.

In this work, we study the morphology of epitaxial (001) $Si_{1-x}Ge_x$ films grown by ultrahigh-vacuum chemical-vapor deposition (UHV-CVD) [3]. The dislocation formation and strain relaxation in these films have previously been studied in detail with transmission electron microscopy (TEM) and X-ray diffraction (XRD) respectively [2, 4, 5]. In addition to providing an ideal test bed for theories of strained layer growth and relaxation, these films have found application for both bipolar and field-effect transistors (FETs) [3]. In the latter case, thick layers with graded Ge concentration are used to form strain-relaxed buffer layers with Ge content near x = 0.30. These buffer layers are then used as substrates for subsequent growth of thin Si layers, forming electron quantum wells surrounded by $Si_{0.7}Ge_{0.3}$ barrier regions [3].

Here we use AFM to obtain a quantitative measure of the surface morphology, which is useful for several reasons. First, for rough films, the AFM provides a detailed measure of facet angles [6], which in turn provides information on the surface free energies in the system, an important factor in strain-induced roughening. Second, for dislocated films, the formation and multiplication of misfit dislocations can be studied by the surface steps which form due to the generation of each individual dislocation [7]. The AFM results complement those obtained by TEM.

Although TEM provides more quantitative information concerning the dislocations, the AFM is a simple tool which can easily be applied to many samples. Finally, the surface roughness information available from Fourier transforms of AFM images is used to deduce limits on electron mobilities in FETs [8].

2. Experimental section

AFM measurements were performed with a Digital Instruments Nanoscope II, in contact mode with a constant net force in the range 30-100 nN, using both Si₂N₄ and pure Si probe tips. These tips have interior angles between sidewalls of 70° and 35° respectively, with the sharper tips used for imaging faceted surfaces (e.g., Figure 2) to avoid tip convolution effects. A problem encountered in contact AFM studies is the presence of large capillary forces due to adsorbed water on the sample, resulting in significant tip wear and/or sample damage. This problem was alleviated by performing all studies in a dry N, atmosphere, and furthermore, by dipping all samples for 5 s in a dilute HF solution prior to imaging, thereby removing the hydrophylic native oxide from the surface. In some cases, AFM measurements were also performed using a Nanoscope III in tapping mode, and good agreement was obtained with the contact mode results. To evaluate limits in the AFM resolution, scanning tunneling microscopy (STM) measurements were performed on selected samples, prepared by HF dipping and immediate introduction into an ultrahigh-vacuum chamber. AFM results were found to have a maximum resolution of about 50 Å, compared to about 10 Å for STM [9]. Overall, the accuracy of the AFM results for roughness amplitude determination is estimated to be $\pm 15\%$, for wavelengths greater than 50 Å [9].

Fourier analysis of the morphology was done using onedimensional (1D) line scans from the images, since this avoids any problems arising from line-to-line scan noise which may be present in the data. To suppress the effects of discontinuities at the endpoints of the line scans, each scan is multiplied by a Hanning function, of the form $C[1 + \cos(2\pi X/d)]$ with -d/2 < X < d/2, prior to the transformation [9]. The constant $C = \sqrt{2/3}$ is chosen to preserve the amplitude squared of each Fourier coefficient, in the limit of high frequencies. Spectra are constructed by averaging the results from typically ten images, acquired over a range of length scales. In the plotted spectra, the Fourier amplitudes are multiplied by the wavevector q, since this removes the 1/q dependence of the amplitudes which typically occurs between roughness components of different lateral length scales.

3. Coherent three-dimensional growth

For a growth temperature near 560°C, and Ge content of $x \approx 0.30$, SiGe films grown on Si(001) substrates are

found to have a rough morphology [6, 10]. This is displayed in Figure 2, for a film with 50 nm thickness. Figure 2(a) shows a conventional representation of the AFM data, with the gray scale in the image determined by the surface height Z(X, Y). The film is seen to be very rough, with the higher regions [white in Figure 2(a)] forming ridges extending along the surface [100] and [010] directions. These ridges are separated by deep pits, which appear dark in Figure 2(a). For rough surfaces it is often useful to plot a derivative of the surface height. One method of selecting a single-valued representation of the two independent derivative values is to consider the surface normal vector $\hat{\mathbf{n}} \equiv (n_x, n_y, n_z) = (-\partial Z/\partial X,$ $-\partial Z/\partial Y$, 1)/c with normalization constant $c = [(\partial Z/\partial X)^2]$ + $(\partial Z/\partial Y)^2$ + 1]^{1/2}, and to take its projection on the average surface normal, $n_z = 1/c$. Figure 2(b) shows this sort of derivative display for the same topography as in Figure 2(a). The elevated ridges in the topography again appear bright in Figure 2(b), since they have relatively small slope (large projection of their surface normal vectors along the Z-axis). The pits exhibit regions of uniformly darker gray, demonstrating the presence of distinct facets, with constant value of slope. Some details of the facets start to appear in Figure 2(b), e.g., thin white lines seen in the pits separate regions with similar slope but different orientation (that is, equivalent facet faces with different orientation).

Quantitative information on the distribution of facets present on the surface can be obtained by forming a twodimensional histogram of the local surface orientations. We display the data as a polar plot, similar to that used in the interpretation of X-ray Laue patterns. The azimuthal angle in the plot equals the azimuthal angle of $\hat{\bf n}$, which is $\tan^{-1}(n_x/n_y)$. The distance of a point from the origin is proportional to the polar angle of $\hat{\bf n}$, which is $\cos^{-1}(n_z)$. With these definitions, the resulting histogram of local surface orientations is shown in Figure 2(c). Points on this polar plot correspond to particular facet orientations on the surface, some of which are labeled in Figure 2(c). We observe broad peaks (FWHM \approx 6°) centered about the four equivalent {105} directions (polar angle of 11.3°). These peaks originate from the ridges between pits, mentioned above, which appear bright in Figures 2(a) and 2(b). In addition, we observe sharper peaks (FWHM $\approx 3^{\circ}$) located at the four {113} directions and the eight {518} directions (polar angles of 25.2 and 32.5°, respectively). Those peaks originate from the sidewalls of the pits, which appear dark in Figures 2(a) and 2(b). The spatial origin of peaks in the histogram is easily determined by placing filters around specified peaks, and transforming back to the Z(X, Y) image to locate the pixels. The result of this procedure is shown in Figure 3, where we have placed filters with diameter of 12° around the sets of {105}, $\{113\}$, $\{518\}$, and $\{5\overline{1}8\}$ peaks in Figure 2. The facets

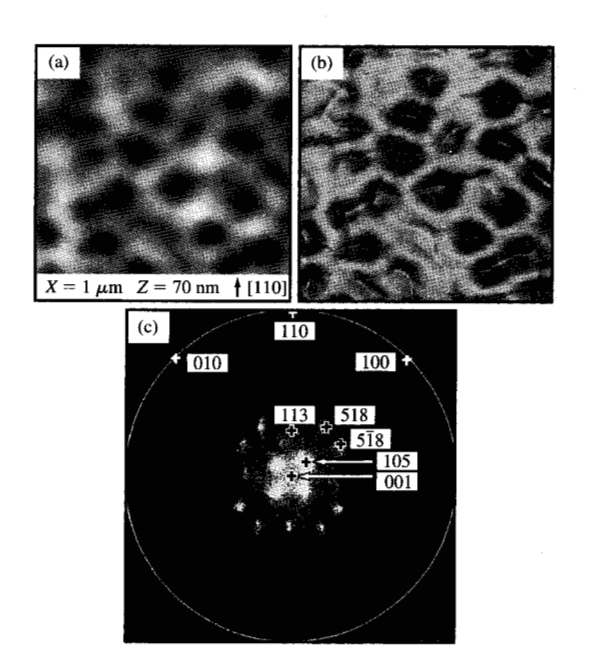


Figure 2

(a) AFM image of 50-nm-thick, x = 0.35 film, grown at 560°C. Gray scale is given by the surface height. Full range values for the scan distance (X) and surface height (Z) are indicated. (b) Same surface topography as (a), displayed in a derivative mode where the gray scale is given by the projection of the local surface normal on the Z-axis. (c) Two-dimensional histogram of orientations of local surface normal $\hat{\bf n}$. Orientations of $\hat{\bf n}$ are displayed as a polar plot, with several orientations indicated by black or white crosses. The large white circle corresponds to a polar angle of $\hat{\bf n}$ of 90°. The gray scale in the histogram is given by the number of observed image pixels with the specified $\hat{\bf n}$ orientation.

corresponding to these peaks are respectively colored red, green, dark blue, and light blue. The distribution of facet angles is now clearly seen in Figure 3, with the facets forming a mosaic or tile pattern on the surface.

The evolution of surface morphology with increasing film thickness has been studied [6]. Islands with typical diameters of 100 nm and height of 12 nm are observed for a thin film with mean thickness of 11 nm. Analysis of the surface orientations reveals polar angles of $\hat{\bf n}$ distributed more or less uniformly over the range 0–13°, with some clustering of the values along azimuthal $\langle 100 \rangle$ directions. For a film with somewhat greater thickness, 20 nm, the SiGe islands are well directed along the surface $\langle 100 \rangle$ directions, and they have formed relatively well-developed sidewalls, described by $\{105\}$ facets. For the 50-nm-thick film pictured in Figures 2 and 3, the surface contains deep pits formed of alternating $\{518\}$ facets, having in an ideal

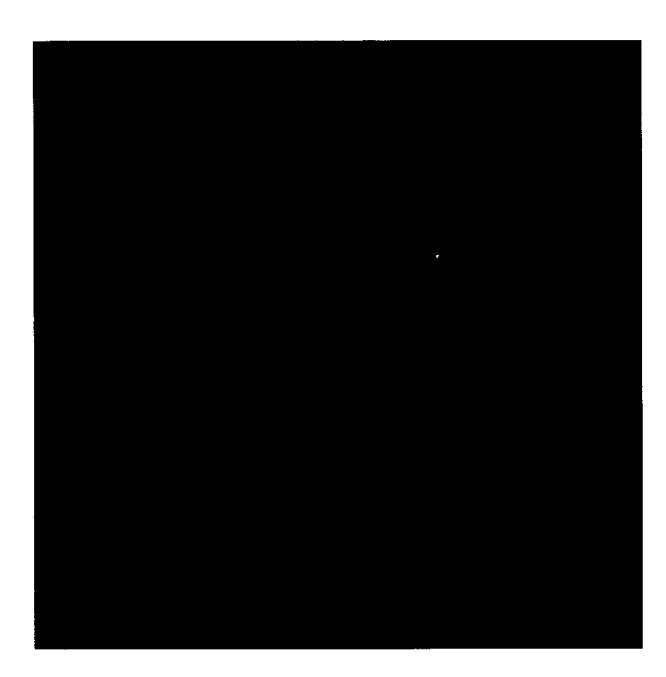


Figure 3

Same image as in Figure 2 colored to illustrate the mosaic arrangement of facets with different orientations. Facet angles clustered within $\pm 6^{\circ}$ of the {105}, {113}, {518}, and {518} directions are colored red, green, dark blue, and light blue, respectively. Regions of the surface with slope not belonging in any of these regions are shaded black in the image.

case eight such sidewalls. These $\{518\}$ facets, being azimuthally oriented nearly along the surface $\langle 100 \rangle$ directions, fit rather well onto the $\{105\}$ faces of the ridges, and we believe this may be a significant factor in their formation. Conversely, the $\{311\}$ facets tend to form in slightly more disordered areas away from the ideal $\langle 100 \rangle$ oriented ridges, since in those areas the $\{311\}$ faces can better achieve their natural $\langle 110 \rangle$ orientation. The $\{311\}$ facets are known to have relatively low energy [11]. The $\{518\}$ facets are observed here for the first time, but from their presence we conclude that they also are energetically favorable. In contrast, $\{508\}$ facets, located on the polar plot between $\{518\}$ and $\{5\overline{18}\}$, must have relatively high energy, since they are not observed here despite their favorable orientation precisely along $\langle 100 \rangle$ directions.

Let us now consider dislocation formation in the films, which partially relieves the biaxial strain arising from lattice misfit between film and substrate. The 11- and 20-nm-thick films mentioned above were found by TEM to have no dislocations. The 50-nm-thick film displayed a substantial number of dislocations, which may have nucleated at the deep pits in the surface morphology [2], and is 15% relaxed as determined by XRD. A 175-nm-thick film was found to contain a high density of dislocations,

and was 86% relaxed. The evolution of morphology changed in that case, with the facets rounding off and the bottom of the pits filling in with (001) faces. This change in morphology is consistent with the removal of the driving force for island and facet formation due to the strain relaxation.

If the surface free energy were isotropic, strain-induced roughening would yield a smoothly corrugated surface with a wavelength determined by the elastic constants of the film and by the mismatch in lattice constant between film and substrate [1, 10]. Facets break the smooth profile into planar segments, but may not otherwise alter the overall morphology very much. In contrast, we believe that the existence of facets has a dramatic effect on the kinetics of strain-induced roughening. With a few discrete facet angles, formation of a corrugated surface requires the nucleation of finite-size protrusions or pits on the surface [2]. The activation energy for this process is highly straindependent, and for sufficiently low mismatch and/or low growth temperature it is expected that strain relief due to dislocation generation will occur before the surface has formed a corrugated morphology. This process of misfit dislocation formation is discussed in the following section.

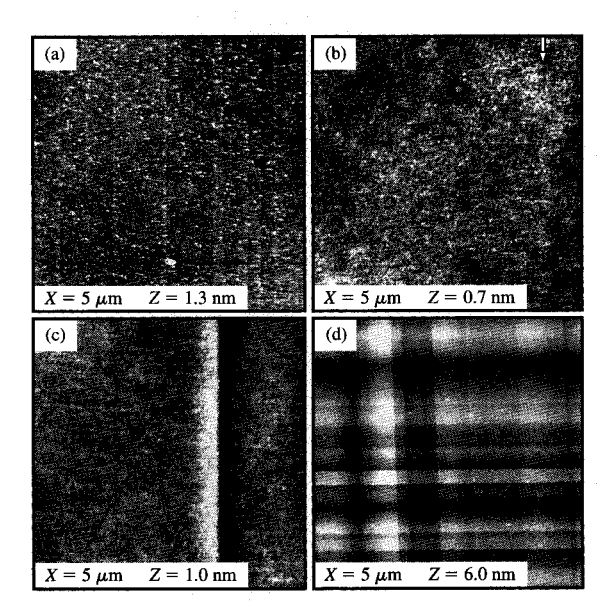


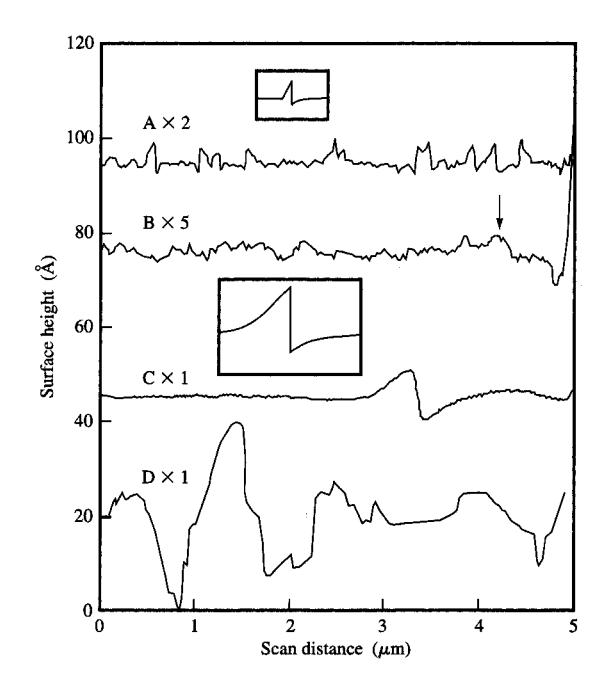
Figure 4

AFM images of $Si_{1-x}Ge_x$ films with x=0.15 Ge content, grown at 560°C. Film thicknesses are (a) 80 nm, (b) and (c) 250 nm, and (d) 400 nm. Full-range values for the scan distance (X) and surface height (Z) are indicated below each image. Individual misfit dislocations are seen in (a), and multiple dislocations are seen in (c) and (d).

4. Misfit dislocations

Since the elastic strain energy in a coherently strained film grows proportional with film thickness, dislocations will eventually form above a critical film thickness to relieve some of this strain. The nature of the misfit dislocations commonly occurring in this system is well known, e.g., from TEM studies [4], and is schematically shown in Figure 1. Their Burgers vectors are $1/2 \langle 110 \rangle$, and they glide on {111} planes. The intersections of these glide planes with the (001) interface plane or with the film surface produce the [110] and [110] directions of the dislocation lines at the interface or atomic-height steps at the surface, respectively. The observation of these surface steps permits a detailed view of the dislocation formation using AFM [7]. In addition to individual misfit dislocations, pileups of 5-10 dislocations lying on the same glide plane are commonly observed by TEM in these films [4]. These pileups are formed by a modified Frank-Read mechanism, in which the intersection points of two perpendicular misfit dislocations with a common Burgers vector act as generation sources for subsequent dislocations.

The formation of misfit dislocations in Si_{0.85}Ge_{0.15} films, grown at 560°C, is illustrated in Figure 4, which shows AFM images of films, with thicknesses of (a) 80 nm, (b) and (c) 250 nm, and (d) 400 nm. Line-by-line background subtraction has been performed on images (a)-(c) (to improve the signal-to-noise ratio), but not for (d). Surface height profiles are shown in Figure 5, obtained by summing all the line scans in each image of Figure 4. Let us first consider results for the relatively thin film of Figure 4(a). Faint white lines are seen there, extending vertically up the image (horizontal lines also exist in the morphology, but are not seen here because of the background subtraction). The height of these lines, as seen in Curve A of Figure 5, is 2.5 \pm 0.3 Å, and their density is 1.5 μ m⁻¹. This density agrees within a factor of 2 with the density of individual misfit dislocations seen in this sample by crosssectional TEM. The steps are thus identified as resulting from the formation of misfit dislocations. Figures 4(b) and 4(c) show the surface morphology of a thicker film. In this case, we do not observe lines with a height of ~ 2.5 Å. Rather, most of the surface is flatter, with very small linear features having a height of ~0.5 Å, one of which is marked by an arrow in Figure 4(b) and Curve B of Figure 5. In addition, we occasionally observe large linear features such as those shown in Figure 4(c) and Curve C of Figure 5. These features have a dipole shape, appearing as a sharp step separating a ridge from a trough, with a step height of 10 Å. The density of these larger features is about 0.2 μm^{-1} , which agrees with the density of dislocation pileups as seen by TEM. We therefore attribute these larger features to the pileups. The surface morphology of a moderately thick film, which is 20% relaxed as determined by X-ray diffraction, is shown in

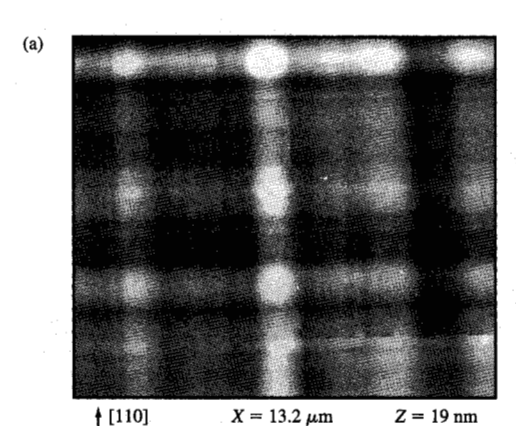


Flaure 5

Surface height profiles, obtained by summing all the line scans in the corresponding images of Figure 4. For Curve D, prior to summation, the image of Figure 4(d) was first rotated by 2.0° to align the observed features accurately along the vertical direction. Insets show theoretical height profiles. The upper inset is for a single dislocation, plotted on the same scale as Curve A. The lower inset is for a pileup of five dislocations distributed uniformly over 0.5 μ m below the film/substrate interface, and is plotted on the same scale as Curve C.

Figure 4(d). We observe a collection of large linear features, of the type identified in Figure 4(c), forming a cross-hatched pattern [these features are seen in Figure 4(d) in both the horizontal and vertical directions, since no line-by-line background has been subtracted]. The density of large features in Figure 4(d), about 2 μ m⁻¹, is in agreement with the density of pileups observed by TEM on this sample.

For comparison with observed surface height profiles, the insets in Figure 5 show computed surface displacements arising from a single 60° dislocation (the Burgers vector is inclined at 60° to the dislocation line) located at the interface or from a pileup of dislocations, respectively. In the upper inset of Figure 5 we show the step, 2.8 Å high, located at the intersection of the glide plane with the surface. Surface displacements on either side of the step are determined by solution of the elasticity equations [12]. The computed curve compares well with the observed profiles in Curve A of Figure 5. The



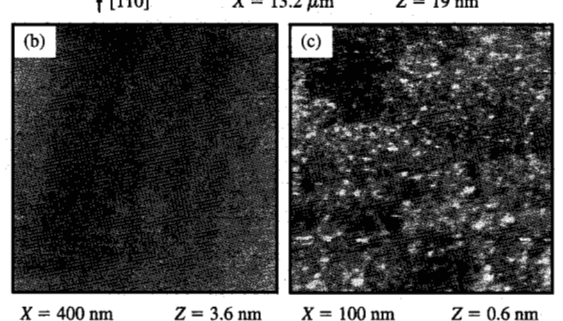


Figure 6

(a) AFM image of 875-nm-thick x = 0.16 film grown at 560°C, displaying large-scale cross-hatched morphology. Expanded views of same sample are shown in (b) and (c), which are STM images displaying atomic-scale roughness on the surface. The lateral (X) and vertical (Z) full-scale ranges are listed below each image.

dislocations can, of course, be oriented with glide planes oriented by either side of the surface normal, and the resulting displacement profiles can have either positive or negative orientation in the scan direction. Also, after formation, the steps may wander because of subsequent film growth. The lower inset in Figure 5 shows the result for a pileup of five dislocations, distributed uniformly over a depth of $0.5~\mu m$ below the film/substrate interface, which is typical of the pileups occurring in this material [4]. The inset is in good agreement with the observed profile in Curve C of Figure 5.

As described above, steps arising from dislocation formation determine the surface morphology of films with thickness $\leq 0.5~\mu m$. Such steps also affect the morphology of thicker films. For example, we have studied an 875-nm-thick Si_{0.85}Ge_{0.15} film which was 88% strain-relaxed, so that it contains 4–5 times more dislocations than the 400-nm-thick film. As pictured in **Figure 6(a)**, the cross-hatched surface morphology of the 875-nm film is significantly

rougher than for the 400-nm film, with peaks and troughs extending over a height range of 150 Å [three to four times that of Figure 4(d)]. The magnitude of the roughness scales with the increased dislocation density, and thus it is consistent with that expected solely from the steps arising from dislocation formation (assuming no step annihilation), but other mechanisms for the cross-hatched formation must also be considered. Morphological changes may also occur due to anisotropic diffusion on the surface induced by the strain from dislocations present in a partially relaxed film [13].

5. Fourier analysis

Quantitative roughness information can be obtained from AFM and STM images by Fourier analysis. This is of particular importance if different types of roughness are present in the surface morphology. Fourier spectra then allow the identification of typical wavelengths and amplitudes for each type of roughness [9]. For example, consider the Si_{0.85}Ge_{0.15} film pictured in Figure 6. As discussed above, cross-hatched morphology is clearly evident in the large-scale AFM image of Figure 6(a). On a much finer scale, atomic steps and disorder lead to another type of roughness, as seen in the STM images of Figures 6(b) and 6(c). In the 400-nm-wide image of Figure 6(b), monoatomic steps can be faintly seen extending roughly vertically up the image. A further expanded view of the surface morphology is shown in Figure 6(c), in which individual monoatomic steps, and other disordered atomic features, are clearly resolved.

The AFM and STM images are Fourier-analyzed according to the procedure described in Section 2, and the results are plotted in Figure 7. We show spectra for the x = 0.16 film of Figure 6, the 50-nm-thick x = 0.35 film of Figure 2, and also a standard commercially available Si substrate. In each case we include results from images of many different sizes (as detailed in Section 2), including both AFM and STM data, and results from the various images are plotted using different symbols. Individual roughness components appear as spectral peaks on this plot. For the x = 0.16 film of Figure 2, we find two spectral peaks, one at a wavelength of 2 µm arising from the cross-hatched pattern, and another at a wavelength of about 50 Å arising from atomic-scale roughness. The Si substrate spectrum reveals a single spectral peak centered at about 100 Å, with amplitude larger than that for the x = 0.16 film (demonstrating that the substrates are slightly rougher than the grown films). The spectrum for the x = 0.35 film reveals a large peak centered at 2000 Å, arising from the island and pit morphology of that rough

We have applied this quantitative roughness analysis to multilayer Si/SiGe heterostructures [8], used for modulation-doped field-effect transistors (MODFETs)

[3, 14]. These structures contain a thick (μm) layer with a graded Ge content of x = 0-0.30, in which the strain is almost completely relaxed by misfit dislocations. On this relaxed Si_{0.7}Ge_{0.3} material, a thin (~100 Å) Si layer is deposited, which is thus under tensile strain and forms a quantum well for electrons, used as a high-mobility electron channel in a MODFET. Several additional thin layers used for supplying electrons to the quantum well complete the structure. AFM images of the surface morphology of such a Si/SiGe heterostructure are shown in Figure 8. In the 10- μ m-wide image of Figure 8(a) a crosshatched pattern is seen, arising from the dislocations and strain fields in the thick layer with graded Ge content. In Figure 8(b), the surface morphology is displayed on an expanded scale. We observe the presence of island and pit features, with lateral extent of 500-1000 Å. We associate the features with 3D growth of the Si channel layer, as for the Si_{0.7}Ge_{0.3} films grown on Si as discussed in Section 3. We note that an orientation analysis [as in Figure 2(c)] of the images of Figure 8 does not yield discrete facets, but

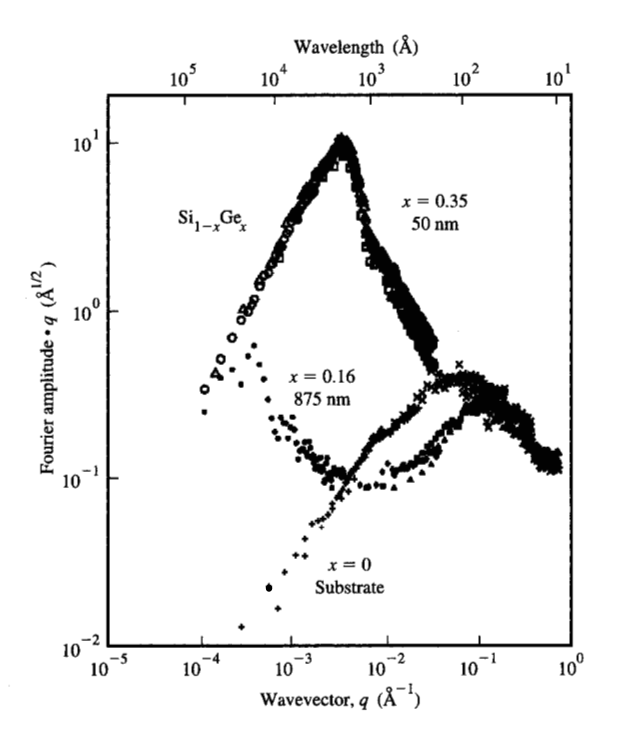


Figure 7

Fourier transforms of the SiGe surface morphology, for Si substrate (+ and × symbols), x = 0.16 film (solid symbols) and x = 0.35 film (open symbols). The Fourier amplitude $|H_q|$, multiplied by the wavevector q, is plotted vs. q. The wavelength $\lambda = 2\pi/q$ is shown on the upper axis. For a given sample, different symbols refer to images of different sizes.

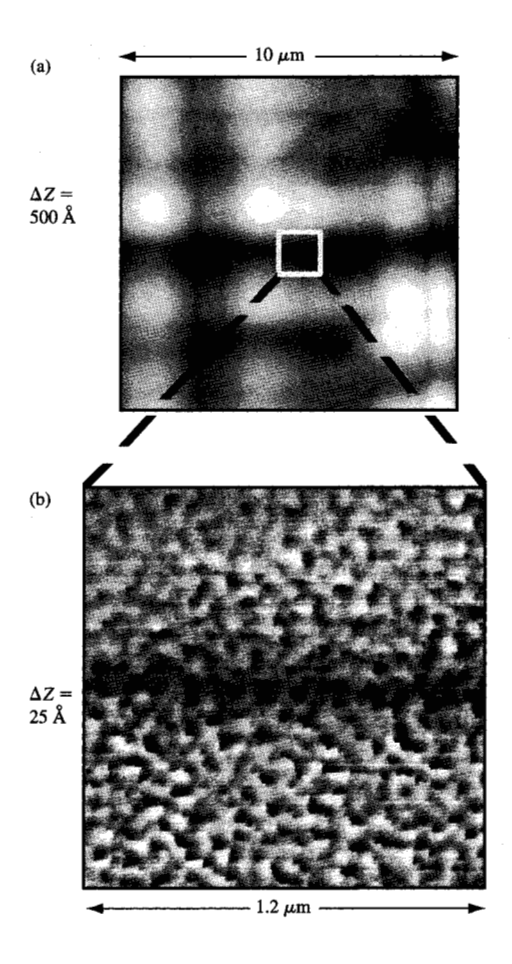
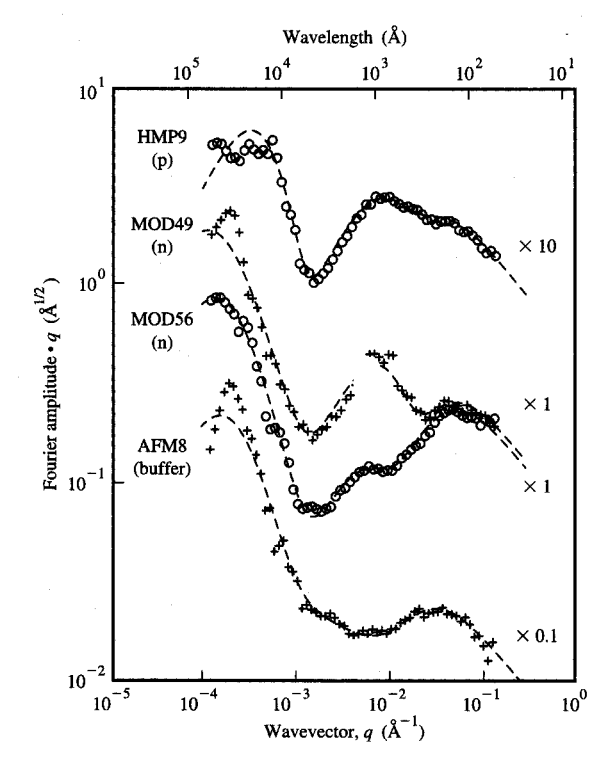


Figure 8

AFM images of a multilayer SiGe device, including a relaxed $\mathrm{Si}_{0.7}\mathrm{Ge}_{0.3}$ layer on which a 100-Å-thick Si quantum well is grown. Surface height is given by a gray scale, with range denoted by ΔZ . For image (b), a local background subtraction has been performed to partially suppress morphology with wavelengths greater than 1000 Å.

instead shows a distribution of surface angles extending out to a few degrees from the cross-hatched morphology, and out to about 10° from the islands and pits.

Fourier spectra of the surface morphology are shown in Figure 9, including results for a variety of different devices, as labeled in the figure. The spectra are seen to consist of three components: a peak centered at a wavelength of 1–2 μ m arising from the cross-hatched morphology, a peak centered at a wavelength of about 1000 Å arising from the island and pit features seen in Figure 8(b), and a peak centered near 100 Å arising from atomic-scale surface roughness. The bottom spectrum in Figure 9, labeled AFM8, was obtained from a structure which did not contain a channel layer, and it does not



Elame 9

Fourier spectra of the surface morphology of various devices. The Fourier amplitude multiplied by the wavevector q is plotted vs. q. The wavelength $\lambda = 2\pi/q$ is shown on the upper axis. For clarity, the spectra are offset from each other by the amounts indicated. The labels HMP9, MOD49, MOD56, and AFM8 refer to different devices which have been studied.

display a clear spectral peak at a wavelength near 1000 Å. This is consistent with the identification of that peak as arising from strain-induced roughness in the channel layer.

On the basis of roughness spectra of the type shown in Figure 9, the effect of roughness at the Si/SiGe interface on the mobility of the electrons in the channel has been evaluated [8]. The inputs to such a computation are the Fourier amplitudes of the roughness spectra, precisely the quantities displayed in Figure 9. For a typical electron density in the channel of $N = 5 \times 10^{11}$ cm⁻², the Fermi wavevector is $k_{\rm F} = (2\pi N/g)^{1/2} = 0.013 \text{ Å}^{-1}$, where g = 2is the number of conduction band valleys for the electrons. The Fermi wavelength is then $2\pi/k_F = 501$ Å, and roughness features with wavelengths of this order will contribute to the scattering. The island/pit features, which are observed in the morphology for wavelengths of 500-1000 Å, as seen in Figure 9, thus constitute an important scattering feature. Detailed mobility computations indicate that for the rougher samples, such

as MOD49 in Figure 9, interface roughness scattering does play a role in determining the low-temperature mobility [8]. For smoother samples, the mobility is limited by other mechanisms, such as scattering by ionized dopant atoms or by misfit dislocations at the Si/SiGe interface [14].

6. Summary

In summary, we have examined the morphology of Si,_,Ge, films using scanning probe techniques. We find that the morphologies reflect the growth mode and subsequent strain relaxation in the films, being either 1) layer-by-layer growth leading to misfit dislocation formation and multiplication, or 2) 3D coherent island growth followed by dislocation formation. A kinetic barrier between these two types of growth is provided by the existence of discrete facets in the surface morphology (anisotropic surface free energy), so that the former mode occurs at reduced strain and/or lower growth temperature. For the layer-by-layer growth, we find that the surface morphology is dominated by steps arising from the dislocation formation. AFM studies of the morphology thus provide useful information on the details of the dislocation arrangement in a film. To quantify the roughness of the Si_{1-x}Ge_x films, we use Fourier analysis, which allows a convenient description of the various types of roughness features occurring on the surface. For the case of Si/SiGe heterostructures, we find that the spectra can be decomposed into three components: μ m-scale cross-hatched, atomic-scale roughness, and island/pit morphology with wavelengths on the 1000-Å scale. These island/pit features are attributed to strain-induced roughening of the channel layer, and this roughness affects the low-temperature mobility of electrons in the channel of MODFET devices.

Acknowledgments

The collaborations of P. M. Mooney, F. K. LeGoues, J. Tersoff, F. Stern, K. Ismail, and B. S. Meyerson in this project are gratefully acknowledged. We also thank N. M. Amer for support and encouragement.

References and note

- D. J. Srolovitz, Acta. Metall. 37, 621 (1989); D. J. Eaglesham and M. Cerullo, Phys. Rev. Lett. 64, 1943 (1990); David Vanderbilt and L. K. Wickham, in Evolution of Thin-Film and Surface Microstructure (MRS Proceedings, Volume 202), C. V. Thompson, J. Y. Tsao, and D. J. Srolovitz, Eds., Materials Research Society, Pittsburgh, 1991, p. 555.
- J. Tersoff and F. K. LeGoues, Phys. Rev. Lett. 72, 3570 (1994).
- 3. B. S. Meyerson, Proc. IEEE 80, 1592 (1992).
- F. K. LeGoues, B. S. Meyerson, J. F. Morar, and P. D. Kirchner, J. Appl. Phys. 71, 4230 (1992).
- P. M. Mooney, F. K. LeGoues, J. O. Chu, and S. F. Nelson, Appl. Phys. Lett. 62, 3464 (1993).

- M. A. Lutz, R. M. Feenstra, P. M. Mooney, J. Tersoff, and J. O. Chu, Surf. Sci. Lett. 316, L1075 (1994).
- M. A. Lutz, R. M. Feenstra, F. K. LeGoues, P. M. Mooney, and J. O. Chu, Appl. Phys. Lett. 66, 724 (1995).
- R. M. Feenstra, M. A. Lutz, F. Stern, K. Ismail, P. M. Mooney, F. K. LeGoues, C. Stanis, J. O. Chu, and B. S. Meyerson, J. Vac. Sci. Technol. B 13, 1608 (1995).
- R. M. Feenstra, M. A. Lutz, and M. Copel, *Mater. Res. Soc. Symp. Proc.* 355, 301 (1995).
- A. J. Pidduck, D. J. Robbins, A. G. Cullis, W. Y. Leong, and A. M. Pitt, *Thin Solid Films* 222, 78 (1992).
- D. J. Eaglesham, F. C. Unterwald, and D. C. Jacobson, *Phys. Rev. Lett.* 70, 966 (1993); D. J. Eaglesham, A. E. White, L. C. Feldman, N. Moriya, and D. C. Jacobson, *Phys. Rev. Lett.* 70, 1643 (1993).
- 12. J. P. Hirth and J. Lothe, Theory of Dislocations, 2nd ed., Krieger Publishing, Malabar, FL, 1992. We consider an incompressible isotropic solid (Poisson ratio of 1/2), and apply the method of image dislocations (p. 86f.). For the displacement normal to the surface (the quantity plotted in Figure 5), we find that the result for the surface case is exactly twice the corresponding displacement in the bulk. The screw component of the dislocation causes no surface displacement.
- J. W. P. Hsu, E. A. Fitzgerald, Y. H. Xie, P. J. Silverman, and M. J. Cardillo, *Appl. Phys. Lett.* 61, 1293 (1992); E. A. Fitzgerald et al., *J. Vac. Sci. Technol. B* 10, 1807 (1992).
- K. Ismail, F. K. LeGoues, K. L. Saenger, M. Arafa, J. O. Chu, P. M. Mooney, and B. S. Meyerson, *Phys. Rev. Lett.* 73, 3447 (1994).

Received February 17, 1995; accepted for publication September 27, 1995

Martin A. Lutz IBM Research Division, Thomas J. Watson Research Center, P.O. Box 218, Yorktown Heights, New York 10598 (malutz@ids.net). Dr. Lutz has worked as a research student at the Thomas J. Watson Research Center and the Zurich Research Laboratory since 1989. He received a Ph.D. degree in 1994 from the Swiss Federal Institute of Technology (ETH) in Zurich, Switzerland. Since then, he has been a postdoctoral fellow in the Physical Sciences Department at Yorktown. Dr. Lutz developed scanning probe microscope instrumentation for surface studies at elevated temperatures and for cross-sectional studies of epitaxial semiconductor structures. His recent research includes the application of STM and AFM for studying Si/SiGe heterostructures, strain-relaxation mechanisms, and the effect of interface roughness on carrier mobility in MODFET devices.

Randall M. Feenstra Department of Physics, Carnegie Mellon University, Pittsburgh, Pennsylvania 15213 (feenstra@andrew.cmu.edu). Dr. Feenstra received his Ph.D. degree in applied physics in 1982 from the California Institute of Technology. He joined the IBM Thomas J. Watson Research Center that year, and spent the next thirteen years studying semiconductor surfaces and heterostructures using scanning probe methods. He developed a number of novel measurement techniques for the scanning tunneling microscope, which were applied to problems of surface-state spectroscopy, chemical specific imaging [resolving Ga and As atoms on the GaAs(110) surface], and observation of surface phase transitions at elevated temperature. In 1995 Dr. Feenstra joined the faculty at Carnegie Mellon, where he is currently studying GaN growth by molecular beam epitaxy. He is a member of the American Physical Society and a fellow of the American Vacuum Society.

Jack O. Chu IBM Research Division, Thomas J. Watson Research Center, P.O. Box 218, Yorktown Heights, New York 10598 (CHUJ at YKTVMV, chuj@watson.ibm.com). Dr. Chu is an advisory engineer in the Electronic Materials and Structures Department at the IBM Thomas J. Watson Research Center. He received a B.S. degree in chemistry from Princeton University in 1978, and M.S. and Ph.D. degrees in chemistry from Columbia University in 1979 and 1984, respectively. He joined IBM at the Thomas J. Watson Research Center as a postdoctoral fellow in 1986 and became an advisory engineer in 1990. Dr. Chu's early work was in the field of chemical dynamics, investigating the gas-phase reactivity of transient species (e.g., SiH₂) relevant to the silicon CVD growth process. More recently, he has been involved in the development and application of the ultrahigh vacuum/chemical vapor deposition (UHV/CVD) technique for fabricating various types of mestastable silicon (Si:Ge, Si:B, SiGe:B, and SiGe:P) alloys and structures with applications to high-performance bipolar and field-effect devices. In particular, high-quality SiGe heterostructures have been fabricated setting world records in the areas of bipolar device performance as well as in modulation-doped FET devices. In 1988, Dr. Chu received an IBM Research Division Award for his contributions to the understanding of silvlene gas-phase dynamics. He recently received an IBM Outstanding Technical Achievement Award for his work on high-mobility electron and hole transport in SiGe structures. Dr. Chu is a member of the American Physical Society.